Microstructural Effects in Face-Centered-Cubic Alloys after Small Charge Explosions

D. FIRRAO, P. MATTEIS, G. SCAVINO, G. UBERTALLI, C. POZZI, M.G. IENCO, P. PICCARDO, M.R. PINASCO, G. COSTANZA, R. MONTANARI, M.E. TATA, G. BRANDIMARTE, and S. PETRALIA

Effects on metal targets after an explosion include the following: fracture, plastic deformation, surface modifications, and microstructural crystallographic alterations with ensuing mechanical properties changes. In the case of small charge explosions, macroscopic effects are restricted to small charge-to-target distances, whereas crystal alterations can still be observed at moderate distances. Microstructural variations, induced on gold-alloy disk samples, as compared to previous results on AISI 304Cu steel samples, are illustrated. The samples were subjected to blast-wave overpressures in the range of 0.5 to 195 MPa. Minimum distances and peak pressures, which could still yield observable alterations, were especially investigated. Blast-related microstructural features were observed on the explosion-exposed surface and on perpendicular cross sections. Analyses using X-ray diffraction (XRD) were performed to identify modifications of phase, texture, dislocation density, and frequency of mechanical twins, before and after the explosions. Optical metallography (OM) and scanning electron microscopy (SEM) observations evidenced partial surface melting, zones with recrystallization phenomena, and crystal plastic deformation marks. The latter marks are attributed to mechanical twinning in the stainless steel and to cross-slip (prevalent) and mechanical twinning (possibly) in the gold alloy.

DOI: 10.1007/s11661-007-9318-z

I. INTRODUCTION

AFTER an explosion, various effects can be observed in a metal target, namely, fracture, gross and localized plastic deformations, surface diffuse modifications of various kinds, and microstructural crystallographic alterations with ensuing mechanical properties changes.[1,2] At some distance from an explosive charge, macro effects vanish; only microstructural variations, such as recrystallization phenomena, intense slip bands or mechanical twins, and possibly phase transformations, are present, with the former to disappear first as distance increases. In the case of small charge explosions, macro effects are restricted to very small charge-to-target distances (on the order of tens of millimeters), whereas at slightly larger distances, most of the variations are of the crystal alteration type. For forensic science investigations, the latter effects are often the only clues remaining after a small charge explosion.

Competition between slip and twins is decided by the value of the stacking fault energy (γ_{sf}) of the metals undergoing explosive shocks. Although previous tests performed with high shock pressures (such as in the pioneering work by Smith[3]) led to evident twinning effects, correlations between the maximum distance of detectability and the shock wave overpressures impinging on a metal object are not found in the literature. Calculations of the maximum shear stress arising from the overpressure at the detectability threshold can be attempted by the use of elasticity theory formulations[4] and the results can be compared with the minimum shear stress necessary to form slip bands or twins.[1] However, experimental proofs of the validity of the approach do not exist.

A comprehensive experimental program has been undertaken to demonstrate the validity of this approach, employing as a target disks of several fcc metals with low to high γ_{sf} values. The results of a series of experiments on 18-carat-gold alloy specimens undergoing explosions at various distances are presented here and are compared with previously reported tests performed on AISI 304Cu specimens and with overpressure measurements performed at various charge-to-target distances.[5,6]

D. FIRRAO, Full Professor, P. MATTEIS, Research Assistant, G. SCAVINO and G. UBERTALLI, Associate Professors, and C. POZZI, Ph.D. Student, are with the Materials Science and Chemical Engineering Department, Turin Technical University, 10129 Torino, Italy. Contact e-mail: donato.firrao@polito.it M.G. IENCO, Associate Professor, P. PICCARDO, Assistant Professor, and M.R. PINASCO, Full Professor, are with the Chemical and Industrial Chemistry Department, Genova University, 16146 Genova, Italy. G. COSTANZA, Assistant Professor, R. MONTANARI, Full Professor, and M.E. TATA, Assistant Professor, are with the Mechanical Engineering Department, Rome "Tor Vergata" University, 00133 Roma, Italy. G. BRANDIMARTE, formerly Director, Explosives Chemistry Institute, Italian Military Navy, is retired. S. PETRALIA, Director, is with Explosives Technology Laboratory, Italian Military Navy, Mariperman, 19138 La Spezia, Italy.

This article is based on a presentation given in the symposium "Dynamic Behavior of Materials," which occurred February 26–March 1, 2007, during the TMS Annual Meeting in Orlando, FL, under the auspices of the TMS Structural Materials Division and the TMS/ASM Mechanical Behavior of Materials Committee.

Article published online September 13, 2007

II. MATERIALS

Four series of disk-shaped specimens, having a diameter equal to 20.5 mm and a thickness, k, equal to 3 mm, have been fabricated by using an AISI 304Cu austenitic stainless steel and an 18-carat-gold alloy.

Two AISI 304Cu bars with the composition reported in Table I (determined by optical emission spectrometry) were used. One bar was annealed at 1060 °C in a protective atmosphere and quenched in oil (small-grain series), whereas the other bar was annealed at 1200 °C in vacuum and gas quenched (large-grain series). Stress relieving for 4 hours at 1050 °C was effected after the disk was cut and polished with a 60-grit paper. Marking and final polishing with emery paper was followed by electrolytic polishing with Struers A2 reactant and 1 minute of electrolytic etching with 10 pct oxalic acid.

Two series of gold-alloy disks were punched from a jeweler production rolled sheet, annealed at 670 °C for 30 minutes (670 series) and at 700 °C for 60 minutes (700 series), and water cooled. The alloy weight percent composition, determined by energy-dispersive spectroscopy (EDS) done on the specimens, was 10.4 ± 0.4 Ag, 14.5 ± 0.1 Cu, balance Au (mean and standard deviation from 7 measures). One face of each specimen was polished (with abrasive papers, diamond paste down to 0.25- and, finally, 0.1-μm colloidal silica) and etched with a KCN-based reactant.

III. EXPERIMENTAL SETUP

The experimental setups are shown in Figure 1. Spherical unconfined charges, consisting of either 50 or 100 g of plastic explosive NSP Bofors Nobelkrut D UN N.0084 (Table II), were exploded in the Italian Navy "P. Cottrau" Proving Ground by cylindrical detonators inserted at their cores. The spherical charges were hung from the detonator electrical cables and the specimens' polished and etched surfaces were placed

Table I. AISI 304Cu Stainless Steel Analysis (Weight Percent)

C	S	P	Si	Mn	Cr	Ni	Mo	Cu	N	Fe
0.015	0.001	0.023	0.41	0.88	17.26	9.16	0.24	3.44	0.017	bal

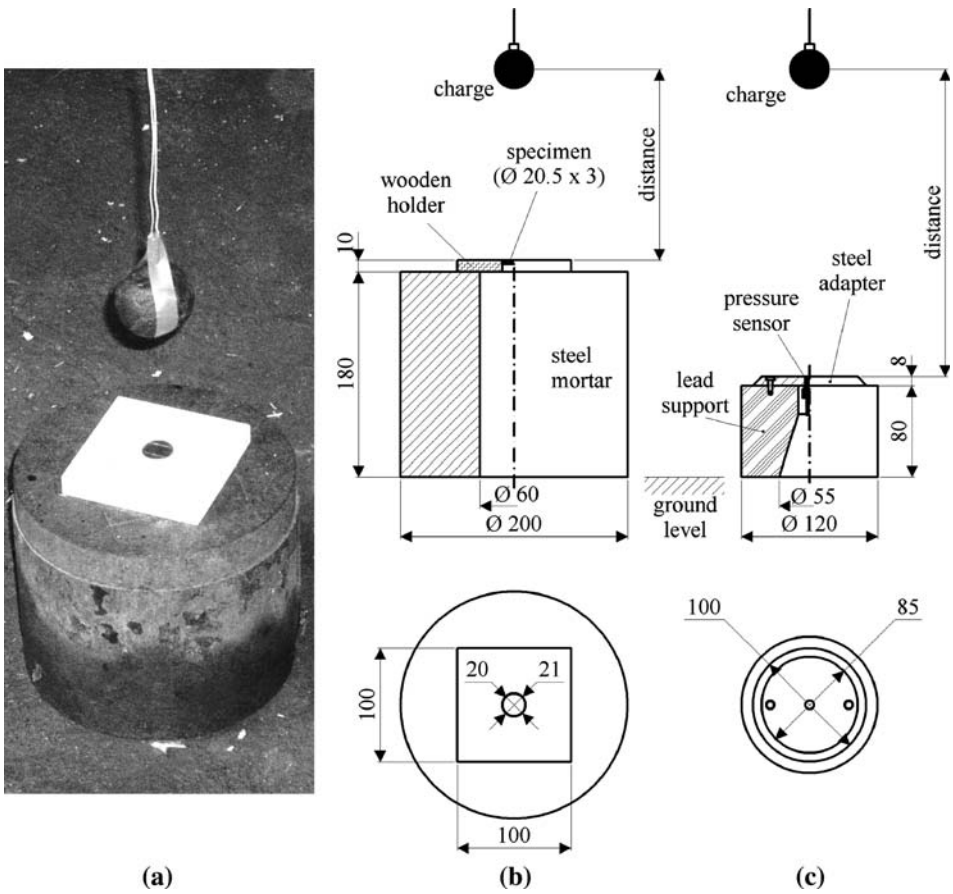

Fig. 1—(*a*) View and (*b*) drawing of experimental setup with metal specimens. (*c*) Drawing of experimental setup with pressure sensors (all dimensions are in millimeters).

Table II. Chemical Analysis of the Explosive (Weight Percent)

Measures by Extraction			Measure from Calcined Residual
Pentrite ($C_5H_8N_4O_{12}$)	Plasticizer (Esters, Naphthenic Oils)	Polymer (Polystyrene, Isoprene)	Carbon Black
86	11	2	0.45

horizontally below the charges (Figures 1(a) and (b)). The trinitrotoluene (TNT) equivalents (determined through the ballistic pendulum, 1.09 mass units of TNT per mass unit of the used explosive) were 54.5 and 109 g, for the 50- and 100-g charges, respectively. The detonators (Figure 2)* consisted of aluminum cases

*Type BRWA 0589.EXP.0867/01, produced by Schaffler & Co., Factory Winzendorf, available from S.E.I. (Società Esplosivi Industriali) s.p.a., It-25016, Ghedi (BS), Italy.

65 mm in length and 7.3 mm in diameter, with less than 1 g of primary and secondary explosive (primary was mixed lead styphnate $C_6HN_3O_8Pb$ and lead azide $Pb(N_3)_2$; secondary was pentrite $C_5H_8N_4O_{12}$).

To approximate free-surface conditions on the face not directly exposed to the shock wave, the specimens were supported only by a very thin circumferential rim of the wooden specimen holders. Destruction of the holders at all distances, but in a few cases at the largest distances, proved that all the specimens have to be considered as unconstrained.

The sample deceleration was not strictly controlled. In most cases, the samples were decelerated against wood chips purportedly positioned inside the steel mortar; in some cases, however, the specimens were deviated (probably due to successive gas waves reflected from the mortar) and finally went on the ground, which consisted of fine sand. In the former case, it can be assumed that the samples were not further modified by the deceleration; in the latter case, some isolated macroscopic scratches were produced on the samples' surfaces. On the basis of the ensuing optical metallography (OM) examinations, the occurrence of a secondary impact against the mortar itself, producing additional generalized effects, was suspected in one case only, with the sample results being taken out from the report.

This experimental setup was preferred to more tightly controlled ones (*e.g.*, involving the use of momentum traps), in order to demonstrate the relevance and usefulness of the ensuing metallurgical analyses in a case as similar as possible to an actual criminal one (*e.g.*, a coin nearby a small bomb).

Stainless steel tests were performed with both charges on the large-grain size; stainless steel tests on the small-grain size and all the gold-alloy tests were effected only with the 100-g charge.

In another series of tests, pressure sensors were placed instead of samples (Figure 1(c)). The pressure sensors (Kistler PCB 102A type) were bonded to a steel adaptor screwed to a lead support, to damp the shock wave when it overtakes the sensor, thus reducing reflections. The charge-to-specimen distances, d, between the center of the prepared spherical charges (30- and 40-mm diameters for the 50- and 100-g charges, respectively) and each specimen's upper surface, were in the 65- to 815-mm interval.

IV. EXPERIMENTAL CALIBRATION

A. *Properties of Blast Waves*

In order to estimate the peak overpressure exercised by the explosion gases (mixed with air) upon the exposed surface (usually defined as reflected pressure, p_r), and the corresponding rise times t_r, in conditions similar to the present experiments, 22 instrumented explosions were performed at distances in the 115- to 335-mm range with 50-g charges and in the 170- to 370-mm range with 100-g charges. The rise times and peak overpressures were obtained from recorded pressure-time curves (0.1-μs sampling); the former were in the 4- to 19-μs range (generally longer for shorter distances, the average being 10 μs), and the latter were in the 11- to 45-MPa range. The overpressure values, p_r, obtained from both the 50- and 100-g charge explosions, were interpolated in respect to the explosion's reduced distances (defined as $r = d \times m^{-1/3}$, where m is the TNT equivalent mass of the charge),** resulting in the

**The reduced distance dependence and the shape of the interpolating function were chosen on the basis of previous theoretical[7] and experimental[8] results.

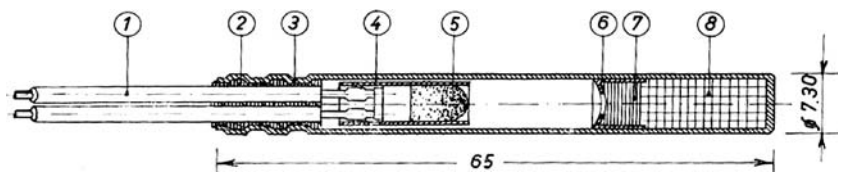

Fig. 2—Detonator, dimensions in millimeters. (1) Copper wires, (2) rubber cap, (3) aluminum case, (4) protective envelope, (5) ignition head, (6) aluminum opening, (7) mixed lead styphnate $C_6HN_3O_8Pb$ and lead azide $Pb(N_3)_2$ primary charge, and (8) pentrite ($C_5H_8N_4O_{12}$) secondary charge.

following expression: $p_r = 13.37/r + 0.141/r^2$, where p_r is expressed in MPa and r is in the range of 0.3 to 0.88 m·kg$^{-1/3}$. This expression was used to calculate the overpressure applied to most of the specimens.

Nevertheless, with the available apparatus, it was not possible to obtain experimental data at reduced distances lower than 0.3 m·kg$^{-1/3}$ (*i.e.*, at overpressure values higher than 46 MPa), whereas the gold-alloy experiments showed some crystal alteration detectability thresholds in the reduced-distance range of 0.19 to 0.29 m·kg$^{-1/3}$. Therefore, the overpressure values in the latter range were estimated both by extrapolating the expression reported here, and by using previously published results. The latter estimate was obtained by first calculating the maximum free-field overpressure, p_d (as a function of the reduced distance, r), from the analytical-experimental formulas from Henrych,[8] and then calculating the corresponding reflected pressure, p_r, at the specimen surface† by using the following correlation (where p_0 is the ambient pressure before the explosion):[9]

$$\frac{p_r}{p_d} = 2 + \frac{6(p_d/p_0)}{(p_d/p_0) + 7}$$

The experimental peak overpressures are presented in Figure 3 as a function of r, alongside the overpressure-*vs*-reduced-distance curves obtained from the interpolation reported here and from the formulas found in the literature and mentioned here. Because the latter curves are significantly different in the reduced-distance range of 0.19 to 0.29 m·kg$^{-1/3}$ mentioned here, it was decided to report both estimates in this range.

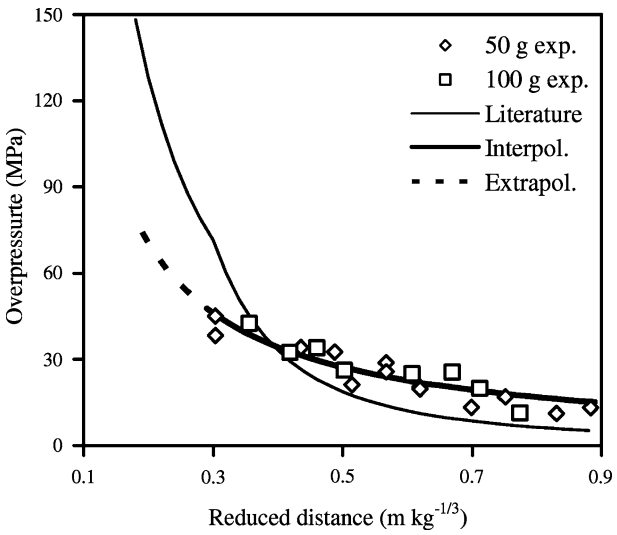

Fig. 3—Computed,[8,9] measured, and interpolated (present results) peak overpressures as a function of the reduced distance, r.

In the ensuing analyses, the blast waves applied on each sample's surface are approximated as plane waves, *i.e.*, the differences in both overpressure and arrival time between the specimen's center (where the overpressure values are calculated) and periphery are neglected, although such an approximation is less valid at the shortest distances.‡ Using the expressions from experimental or literature expressions reported here to calculate $p_r(r)$, the peak overpressure difference between the center and the periphery of the sample is less than 2 pct at the shortest distances, as computed on the basis of the distance of each point from the charge center, and rapidly vanishes with increasing distance. Nevertheless, a lower reflected overpressure may be hypothesized close to the specimen's periphery, because in this position the expansion of the explosion gases is less hindered than on most of the specimen's surface; for this reason, the subsequent observations were generally performed in the specimen's central region and, in any case, not close to the specimen's periphery.

B. *Specimen Stress Histories*

In the case of experiments with charge-to-target distances close to or larger than the microstructural variation detectability thresholds, and resulting in negligible or nil final plastic deformation, the specimen's stress history can be estimated by using the (dynamic) elasticity theory. Moreover, because the specimen has a low thickness-to-diameter ratio, the uniaxial deformation approximation can be employed, leading to the following analytical solution (without attenuation) for the first principal stress σ_{11}:

$$\sigma_{11} = \sum_{n=0}^{n<\frac{V\cdot t+x}{2k}} \left\{ p\left(t - \frac{k\cdot(2\cdot n+1)+(k-x)}{V} \right) \right\} - \sum_{n=0}^{n<\frac{V\cdot t+x}{2k}} \left\{ p\left(t - \frac{k\cdot(2\cdot n)+(x)}{V} \right) \right\}$$

where x is the position inside the specimen, located between zero (the surface subjected to the pressure, p_r) and k (the free surface), V is the uniaxial-deformation sound speed,§ t is the time, and $p_r(t)$ increases from zero at $t \le 0$ to its maximum value at $t = t_r$. This solution can be interpreted as a sum of positive and negative waves, traveling in the forward and backward directions, respectively, each having the same shape of $p_r(t)$. The first positive wave is directly produced by the externally applied pressure $p_r(t)$, whereas the others are produced by successive reflections at the specimen surfaces.

†The reflected overpressure p_r is higher than the free-field overpressure p_d, because the specimen surface hinders the gas expansion.

‡For this reason, most OM observations (especially at the lower charge-to-sample distances) were made close to the sample center.

§V is equal to $\sqrt{(E\cdot(1-\nu)/(\rho\cdot(1+\nu)\cdot(1-2\cdot\nu)))}$, E being the Young modulus, ν the Poisson coefficient, and ρ the density.

By calculating the previous equation, it can be shown that the stress profiles and stress histories inside the specimen depend critically upon the $2 \times k/V$ duration, which is the time employed by a uniaxial-deformation wave to travel twice through the specimen. This duration is about 1 and 2.8 μs for the stainless steel and gold-alloy specimens, respectively (as obtained from data in the literature on density and elastic properties), *i.e.*, it is always shorter, and in most cases much shorter, than the rise times, t_r, mentioned here. As a consequence, when the first negative wave reaches the exposed surface (at $t = 2 \times k/V$), the overpressure $p_r(t)$ applied to the same surface has not yet reached its peak value, and thus, due to the destructive interference between the positive and negative waves, such a peak value cannot be reached at points different from the exposed surface itself (Figure 4(a)). Afterward, several (positive and negative) reflected waves are contemporaneously active, but their superposition produces a pressure profile that (at any given time instant) decreases monotonically from the exposed surface (where $\sigma_{11} = -p_r$) to the free surface (where $\sigma_{11} = 0$; Figure 4(a)), and a stress history that (in any point inside the specimen) consists of only one significant pressure rise and pressure decrease (plus many negligible oscillations; Figure 4(b)), with an overall maximum value that decreases with the distance from the exposed surface; no relevant negative pressure (*i.e.*, tension) occurs.

Therefore, in the cases mentioned here, the eventual microscopic modifications observed after the explosion in any point in the specimen are due to a single load peak.

Moreover, since the analysis described here may not be valid at the shortest distances, where sensible plastic deformation occurs, and since, consequently, the calculation of the maximum load occurring at points inside the specimen would be more uncertain in these cases, all the reported observations were made either on the exposed surface itself or in the cross section close to the exposed surface.

V. RESULTS

A. *Specimen Deformation*

The specimens' deformation has been evaluated by measuring their thickness before and after the explosions with a micrometer caliper (instrumental uncertainty of $\pm$ 0.01 μm).

The thickness of the AISI 304Cu steel disks was not modified by the explosions, except for specimens very close to the charges, which showed either a slight decrease owing to compression (50-g charges) or a slight increment due to the melting of large portions of the surfaces (100 g). At charge-to-specimen distances larger than 115 mm (50-g explosive charges) or 170 mm (100-g charges), no macroscopic deformation was detected, thus revealing that general yielding was not reached (Tables III, IV, and V).

It was not always possible to measure univocally the deformation of the gold-alloy disks, because of relevant planarity defects due to the presence of large surface melting and resolidification areas (Tables VI and VII). Significant deformations (up to 5 pct in the large-grain series) were measured in the 700-series disks subjected to 100-g charge explosions at the smallest tested distances (70 to 110 mm). On the contrary, the 670-series disk subjected to a 100-g charge explosion at a distance of 70 mm showed a deformation of 1 pct only, but no other measurement at distances smaller than 170 mm was available to confirm this result. In both series, the deformations were negligible at distances larger than 170 mm.

Therefore, at distances above the reported limits, the elasticity theory can be applied to transform surface overpressures into surface-applied shear stresses.[1,4]

B. *Hardness*

The specimens' hardness was measured before and after the explosions. After the explosions, the microhardness of most of the stainless steel specimens was

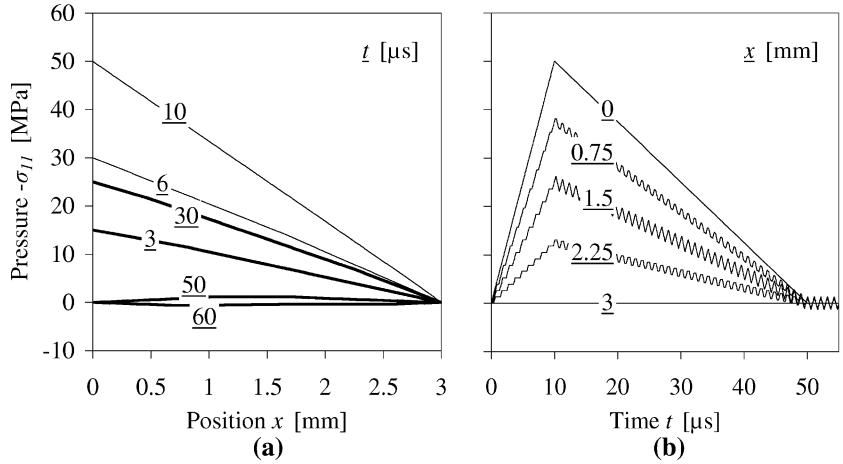

Fig. 4—Calculated pressure in the blast-exposed specimens: (*a*) pressure-*vs*-position curves at given times *t* and (*b*) pressure-*vs*-time curves at given positions *x*. Uniaxial deformation model, triangular waveform with representative rise time (10-μs) and positive time (50-μs) values.

Table III. AISI 304Cu: Results of the Large-Grain, 50-g Charge Experiments

No.	d (mm)	Reduced Distance (TNT Equivalent) ($m \cdot kg^{-1/3}$)	p_r Interpolated (MPa)	τ_{max} (MPa)	Deformation (mm)	Deformation (Pct)	Crystal Deformation Marks (OM) (Surface)	Crystal Deformation Marks (OM) (Section)
8	65	0.17	—	—	−0.05	−1.6	*	yes
22	65	0.17	—	—	−0.04	−1.3	yes	yes
12	75	0.20	—	—	0	0.0	yes	yes
23	85	0.22	—	—	−0.02	−0.7	yes	yes
10	95	0.25	—	—	−0.01	−0.3	yes	yes
30	115	0.30	45.6	23.5	0	0.0	yes	no
2	135	0.36	38.6	19.9	0	0.0	yes	no
25	165	0.44	31.5	16.2	0	0.0	yes	no
19	195	0.51	26.5	13.7	0	0.0	yes	no
13	215	0.57	24.0	12.4	0	0.0	no	no
6	415	1.09	—	—	0	0.0	no	no
9	815	2.15	—	—	0	0.0	no	no

*Not observable.

Table IV. AISI 304Cu: Results of the Large-Grain, 100-g Charge Experiments

No.	d (mm)	Reduced Distance (TNT Equivalent) ($m \cdot kg^{-1/3}$)	p_r Interpolated (MPa)	τ_{max} (MPa)	Deformation (mm)	Deformation (Pct)	Crystal Deformation Marks (OM) Surface	Crystal Deformation Marks (OM) Section
17	120	0.25	—	—	0.04	1.3	yes	yes
18	140	0.29	—	—	0.02	0.6	yes	yes
4	170	0.36	38.7	19.9*	0.01	0.3	yes	yes
20	200	0.42	32.7	16.9	0	0.0	yes	no
3	220	0.46	29.7	15.3	0	0.0	yes	no
21	240	0.50	27.2	14.0	0	0.0	yes	no
24	270	0.57	24.1	12.4	0	0.0	no	no
7	420	0.88	15.4	7.9	0	0.0	no	no

*Invalid due to plastic deformation.

Table V. AISI 304Cu: Results of the Small-Grain, 100-g Charge Experiments

No.	d (mm)	Reduced Distance (TNT Equivalent) ($m \cdot kg^{-1/3}$)	p_r Interpolated (MPa)	τ_{max} (MPa)	Deformation (mm)	Deformation (Pct)	Crystal Deformation Marks (OM) Surface	Crystal Deformation Marks (OM) Section
A02	100	0.21	—	—	0	0.0	yes	yes
A16	120	0.25	—	—	0.03	1.0	yes	yes
A17	140	0.29	47.2*	24.4†	0.02	0.7	yes	yes
A01	170	0.36	38.7	19.9†	0.01	0.3	yes	no
A05	200	0.42	32.7	16.9	0	0.0	yes	no
A04	220	0.46	29.7	15.3	0	0.0	yes	no
A14	240	0.50	27.2	14.0	0	0.0	yes	no
A15	270	0.57	24.1	12.4	0	0.0	no	no
A07	320	0.67	20.3	10.4	0	0.0	no	no

*Slightly extrapolated.
†Invalid due to plastic deformation.

measured on the exposed surfaces, in areas far away from both surface melting and fragment impact. In some stainless steel specimens and in most gold-alloy specimens, such a measure was not possible because of the dearth of areas that were free from these surface alterations and that were sufficiently large and plane.

Table VI. 18-Carat-Gold Alloy: Results of the 670 Series, 100-g Charge Experiments

Number	d (mm)	Reduced Distance (TNT Equivalent) ($m \cdot kg^{-1/3}$)	p_r (MPa)	τ_{max} (MPa)	Deformation (mm)	Deformation (Pct)	Crystal Deformation Marks (OM) Surface	Crystal Deformation Marks (OM) Section
Au670_3	70	0.15	—	—	–0.03	–1.0	†	yes
Au670_1	90	0.19	74.3* (140**)	14.2*‡ (26.9**)‡	—	—	yes	yes
Au670_2	110	0.23	60.8* (106**)	11.6*‡ (20.3**)‡	—	—	yes	no
Au670_5	130	0.27	—	—	—	—	yes	no
Au670_7	150	0.31	44.3	—	—	—	yes	no
Au670_4	170	0.36	38.7	—	–0.02	–0.7	yes	rare
Au670_10	170	0.35	39.1	—	—	—	yes	rare
Au670_6	200	0.42	32.7	6.3§	–0.03	–1.0	yes	rare
Au670_9	240	0.50	27.2	5.2	0	0	no	no

†Not observable due to surface melting.
*Extrapolated/from extrapolated p_r.
‡Invalid due to plastic deformation or surface melting.
**Empirical formulas from literature.
§Invalid due to plastic deformation.

Table VII. 18-Carat-Gold Alloy: Results of the 700-Series, 100-g Charge Experiments

No.	d (mm)	Reduced Distance (TNT Equivalent) ($m \cdot kg^{-1/3}$)	p_r Interpolated (MPa)	τ_{max} (MPa)	Deformation (mm)	Deformation (Pct)	Crystal Deformation Marks (OM) Surface	Crystal Deformation Marks (OM) Section
Au700_1	70	0.15	—	—	–0.16	–5.4	†	yes
Au700_2	90	0.19	74.3* (139**)	14.2*‡ (26.6**)‡	–0.13	–4.4	yes	yes
Au700_3	110	0.23	60.8* (105**)	11.6*‡ (20.1**)‡	–0.15	–5.2	yes	rare
Au700_6	130	0.27	51.5* (82**)	9.8*‡ (15.8**)‡	—	—	yes	no
Au700_8	150	0.31	44.0	—	—	—	yes	no
Au700_4	170	0.36	38.7	—	–0.09	–3.1	yes	no
Au700_7	200	0.42	32.7	—	–0.01	–0.3	yes	no
Au700_9	220	0.46	29.7	5.7§	–0.01	–0.4	yes	rare
Au700_5	320	0.67	20.3	3.9	—	—	no	no

†Not observable due to surface melting.
*Extrapolated/from extrapolated p_r.
‡Invalid due to plastic deformation or surface melting.
**Empirical formulas from literature.
§Invalid due to plastic deformation.

Thus, in the gold-alloy specimens, after the explosions, the microhardness was measured in the sections close to the exposed surface, in areas containing parallel marks (in those specimens that showed such features).

Regarding the stainless steel, the hardness of the as-fabricated large-grain and small-grain specimens was 114 and 116 $HV_{0.1}$, respectively; a limited hardness increase, up to 136 $HV_{0.1}$, was detected in specimens of both the large- and small-grain series exposed to blast waves with target-to-charge distances lower than 100 and 180 mm, respectively, for the 50-g and 100-g charges. The increase was generally larger for specimens subjected to higher stresses.

On the other hand, in the gold-alloy series, the hardness (161 and 171 $HV_{0.1}$ in the as-fabricated 700 and 670 series, respectively) showed only a very small decrease, of less than 5 HV units in each series, perhaps due to the heat wave. Because this variation was just noticeable in respect to the measurement uncertainty, it was not possible to correlate it with the charge-to-target distance.

C. *Microstructures*

The original microstructure of both the stainless steel and the gold alloy, as visible by OM, showed polygonal grains with frequent large recrystallization twins (Figure 5). Precipitates (or cavities consequent to their extraction) were observed in the stainless steel along the polygonal boundaries, but not along the twin boundaries. The two groups of stainless steel specimens presented 60- and 32-μm average grain sizes after annealing at 1200 °C and 1060 °C, respectively. The corresponding values in the gold-alloy specimens

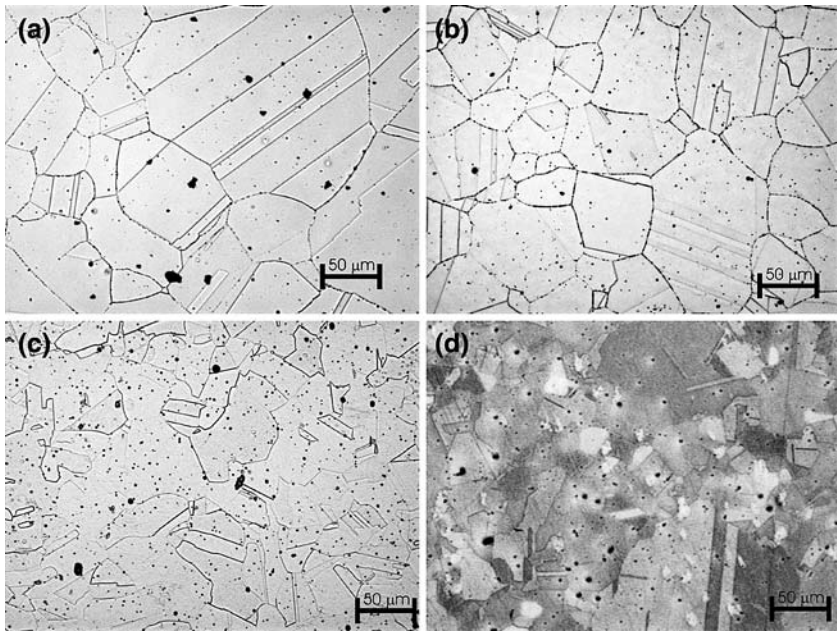

Fig. 5—Original microstructures: AISI 304Cu stainless steel with (*a*) large, 60-μm and (*b*) small, 32-μm grains (OM with electrolytic 10 pct oxalic acid etching); gold-alloy (*c*) 700 series with 55-μm grains; and (*d*) 670 series with 46-μm grains (OM with KCN base reactant etch).

annealed at 700 °C and 670 °C were 55 and 46 μm, respectively.

The modifications of the exposed surfaces, observed after the explosions by OM and scanning electronic microscopy (SEM), in different cases, include the following: melting and resolidification, either complete or partial (at grain boundaries or upon limited areas); impact craters with deposition of oxidized explosive components and of material originated from detonator case fragments; and a series of crystal plastic deformation parallel marks (possibly crossed) limited by the grain boundaries.

Some areas affected by melting were observed by low-magnification OM (Figure 8(f)) and by SEM; the oxidation was verified by EDS on a stainless steel specimen. The melted and resolidified layer was examined by OM in the cross section of the two gold-alloy specimens exploded at the smaller distance: its thickness was estimated between 0 and 6 μm in the 700-series samples, and between 6 and 13 μm in the 670-series samples (in different points), although it was not possible to resolve single grains inside it. Similarly, some isolated line-up of small grains adjacent to the exposed surface were observed in the cross sections of the stainless steel specimens, even if their correspondence with the melted areas could not be proved unambiguously (*e.g.*, Figure 6(c)). The melting and resolidification phenomenon occurred in most gold-alloy specimens and in some stainless steel specimens subjected to the explosions at the smaller distances, but was in most cases inhomogeneous, with several squared-millimeter-wide areas either completely affected or completely unaffected; the OM analysis of the unaffected areas showed the other features mentioned here, especially the parallel crystal plastic deformation marks.

In addition to the melted layer mentioned here, the modifications observed by OM in the metallographic sections perpendicular to the exposed surfaces, cut by electrical discharge machining (EDM) after the explosions, were generally restricted to a similar series of parallel crystal plastic deformation marks occurring in a limited layer adjacent to the exposed surface.

The crystal plastic deformation parallel marks were evident in regions where, apparently, the original grain boundaries and annealing twin boundaries had not been altered by the blast waves. The marks were always limited by the grain boundaries and limited or deviated by the annealing twin boundaries. Two intersecting series of parallel marks often occurred in the same grain, and three intersecting series occurred in very few cases; at these intersections, the marks were not sensibly deviated or displaced.

The parallel marks observed on the exposed surfaces were planarity variations of the original polished and etched surface, directly due to the deformation caused by the shock wave, whereas those observed on the perpendicular sections resulted from the metallographic etch performed after explosions and cross sectioning; thus, these marks may give evidence of the same physical phenomena, with different effectiveness in the two cases.

The parallel marks are generally interpreted as the traces of either mechanical twin planes, slip planes (a cross-slip behavior can be hypothesized in some instances), or a combination of both.

The parallel marks were much more evident through the OM than through the SEM, particularly for those observed on the sections. On the exposed surfaces, the parallel marks were generally more frequent and evident around the fragment impact points mentioned

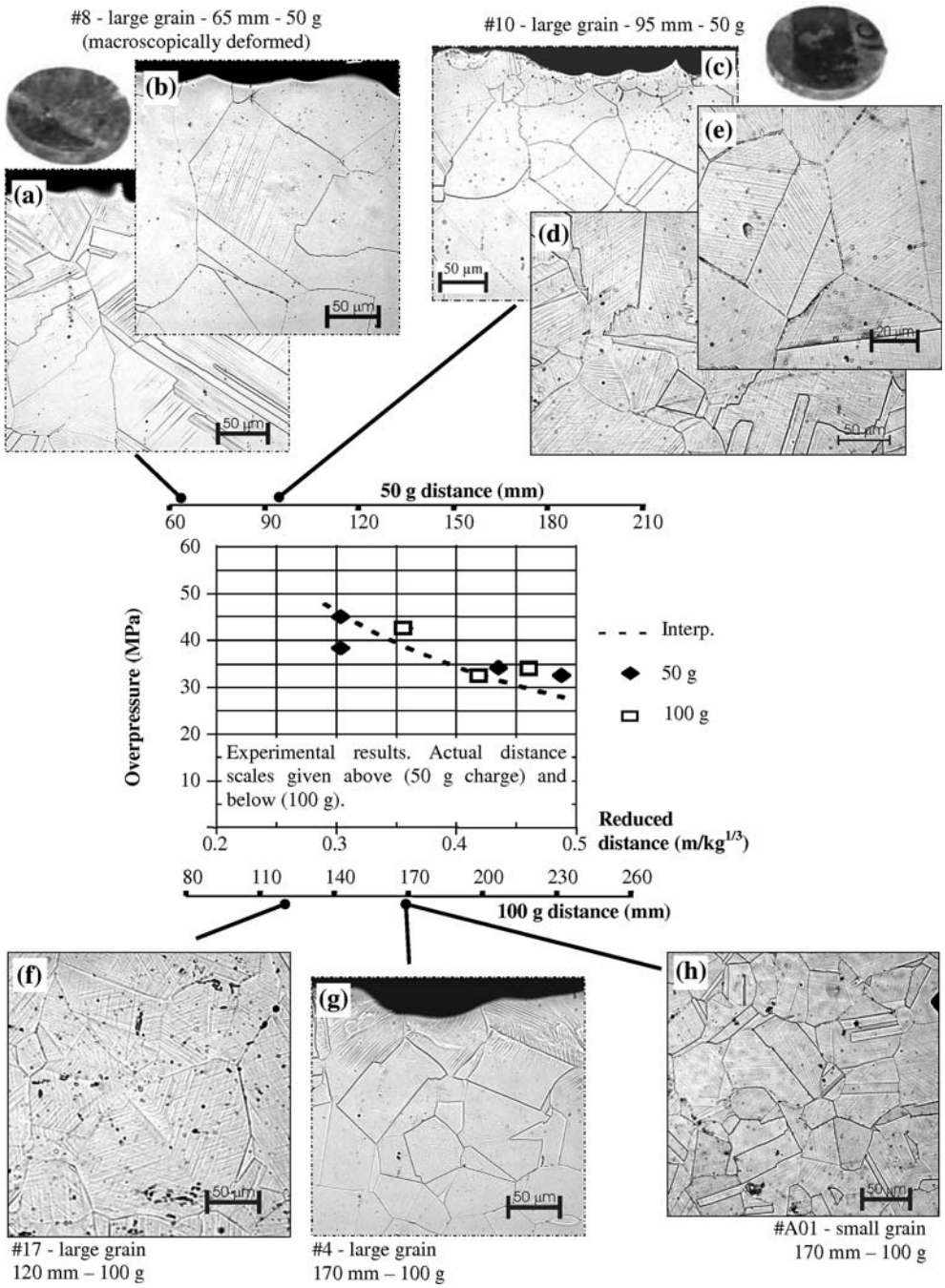

Fig. 6—Microstructural OM observations of blast-exposed AISI 304Cu specimens compared to the experimental overpressure-distance curve; reduced distance in the 0.2 to 0.5 $m \cdot kg^{1/3}$ range (original surfaces and cross sections).

here, and were observed at these particular points even in specimens subjected to explosions at the larger distances, in which they were elsewhere absent (Figure 7(b), hereafter).

The effect of the reduced distance in determining the occurrence of microstructural changes is clearly demonstrated by Figure 6, in which surface and cross section modifications in stainless steel samples are grouped for the smallest values of reduced distance, and by Figure 7, in which the analogous features are reported for the larger values of reduced distance; the same phenomenon can be appreciated in Figure 8, in regard to the gold-alloy specimens. At the lower reduced distances, the parallel marks occupy the total of the exposed surface (with the exception of the eventual melting and resolidification areas) as well as of the grains inside a discontinuous layer adjacent to the surface (observed in the cross sections); by increasing the reduced distance, the parallel marks are gradually less evident and, finally, are limited to areas around fragment impact points or

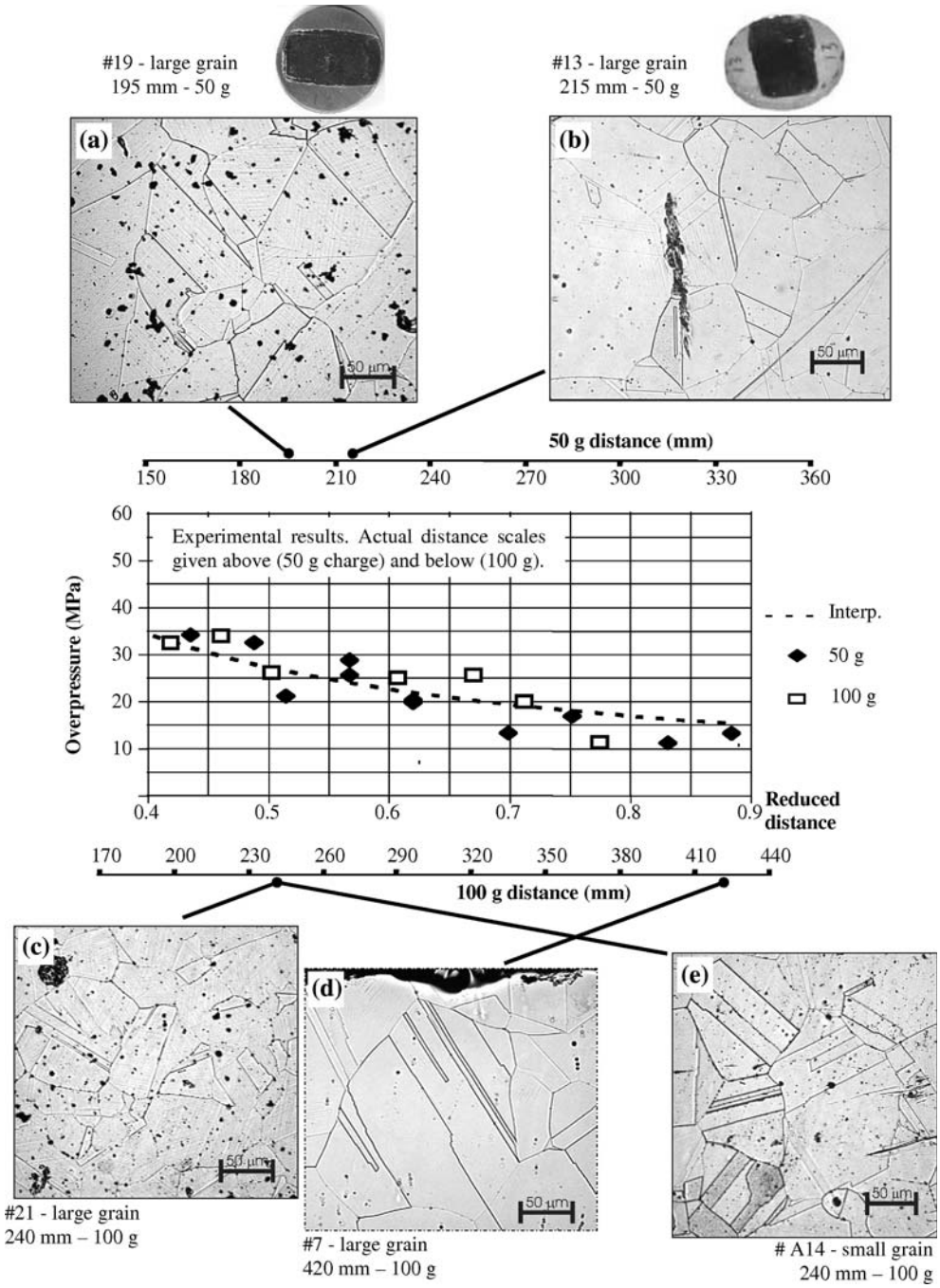

Fig. 7—Microstructural OM observations of blast-exposed AISI 304Cu specimens compared to the experimental overpressure-distance curve; reduced distances in the 0.4 to 0.9 m/kg$^{1/3}$ range (original surfaces and cross sections).

are very rare, short, and shallow and restricted to a few isolated grains.

The experimental results are listed in Tables III through VII; the occurrence of parallel crystal marks both upon the whole exposed surface and in the section (in the mostly limited layer adjacent to the exposed boundary) is evidenced. Table VIII summarizes, for each series of specimens, the threshold distances for the observation of crystal deformation marks either on the whole exposed surface or in the cross-section layer mentioned earlier. Immediately below the listed surface thresholds, the surface crystal deformation marks are just noticeable but are still extended to all grains, whereas above the same thresholds, only rare isolated marks were observed on the surfaces. In the sections, the maximum thickness of the layer containing parallel marks rapidly decreases with increasing distance and not even a partially continuous layer was observed at distances equal to or larger than those listed in Table VIII.

Because both twinning and slip result from an applied shear stress, the maximum surface shear stresses have

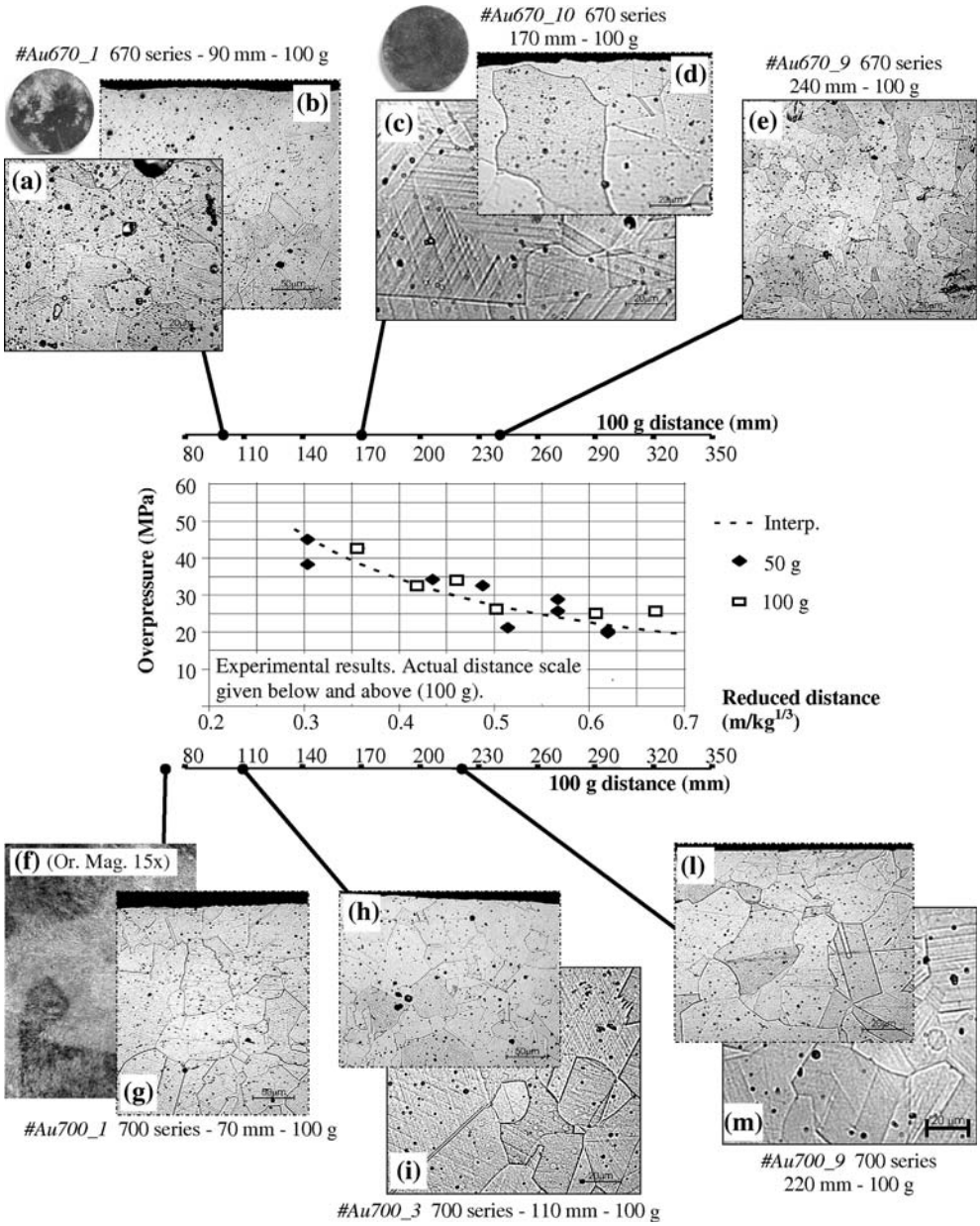

Fig. 8—Microstructural OM observations of blast-exposed 18-carat-gold-alloy specimens compared to the experimental overpressure-distance curve (original surfaces and cross sections).

been reported for distances above the gross deformation annihilation. The shear stress values were computed from the reflected pressure values (derived from the empirical formulas reported earlier or from the experimental results) by applying the previously justified hypothesis of elasticity. In most cases, this hypothesis is valid at distances close to or larger than the OM detectability thresholds. Nevertheless, in some cases, limited plastic deformation or partial surface melting occurred at the OM detectability thresholds; in these cases, the shear stress values calculated with the same method are also reported in Tables III through VII, and in Table VIII for comparison, although they are not completely valid.

D. *X-Ray Diffraction Analysis*

The X-ray diffraction (XRD) analysis was performed on the exposed surfaces of the as-prepared and blast-exposed samples, in order to identify modifications concerning the phases, the texture, the crystallite size, and the densities of dislocations, stacking faults, and twin planes, before and after the explosions. In regard to the stainless steel specimens, overall diffraction patterns (5- to 60-deg 2θ angular range, 0.05-deg steps, and 2-s/step counting time) and precision peak profiles of the 111, 200, 220, 311, and 331 reflections (0.005-deg steps and 10-s/step counting time) were collected employing the Mo K_α radiation. The overall diffraction patterns

Table VIII. Threshold Distances and τ_{max} Values for Detection of Explosion-Related Crystal Deformation Marks

		Whole Surface Marks		Section Layer Marks	
		Distance (mm)	τ_{max} (MPa)	Distance (mm)	τ_{max} (MPa)
AISI 304Cu 60 μm, 50 g	observed	195	13.7	115	23.5[§]
	not observed	215	12.4	135	19.9
AISI 304Cu 60 μm, 100 g	observed	240	14.0	170	19.9[§]
	not observed	270	12.4	200	16.9
AISI 304Cu 32 μm, 100 g	observed	240	14.0	140	24.4[†§]
	not observed	270	12.4	170	19.9[§]
18 carat gold 670 series, 100 g	observed	200	6.3§	90	14.2[†§] (26.9**)[§]
	not observed	240	5.2	110	11.6[†§] (20.3**)[§]
18 carat gold 700 series, 100 g	observed	220	5.7[§]	90	14.2[†§] (26.6**)[§]
	not observed	320	3.9	130	9.8[†§] (15.8**)[§]

[§]Invalid due to plastic deformation or partial surface melting.
[†]From extrapolated experimental reflected pressure.
**Empirical formulas from literature.

(10- to 60-deg 2θ angular range, 0.05-deg steps, and 2-s/step counting time) and precision peak profiles of the 111, 200, and 220 reflections (0.005 deg and 10 s/step) of most gold-alloy specimens were collected by Mo K_α radiation. Overall diffraction patterns (30- to 110-deg 2θ range, 0.1-deg steps, 5-s/step counting time) and precision peak profiles of the 111, 200, and 220 reflections (0.004-deg steps, 5-s/step counting time) were also performed by Co K_α radiation on as-prepared samples, of both gold-alloy series.

Because the employed X-ray spot covers an area on the order of 10 mm^2, and because the specimens' exposed surface were generally inhomogeneous, the XRD analysis generally averages the pointwise effects (*e.g.*, those due to fragment impacts) with the generalized ones, and also averages the regions having different characteristics (*e.g.*, subjected or not subjected to surface melting), that the OM analysis reported earlier examined separately. In particular, by considering the X-ray absorption coefficient of the present gold alloy, the fractions of the integrated X-ray intensity between the surface, and the already mentioned 6- and 13-μm observed depths of the melted layer are 61 and 87 pct of the total integrated intensity, respectively. Therefore, even if the melted layer were thinner in other specimens and points, it can be safely concluded that the XRD signal obtained from a melted and resolidified area bears a large contribution of the melted material, as opposed to that of the underlying unmelted (but possibly microscopically deformed) material. Moreover, because the ratio of melted and unmelted surface areas and the number of fragment impacted points that together make up the X-ray spot was substantially random, any estimate of the features mentioned here (particularly the crystallite size and the densities of linear and planar defects) that can be obtained from the XRD results is expected to be affected by a large uncertainty and a dispersion of results.

Given this, the decision was made to analyze the diffraction patterns and the precision peak profiles qualitatively and on the basis of descriptive parameters only (such as the position of the maximum and the full width at half height, obtained either directly or after fitting with empirical functions), rather than by using the more advanced full-profile fitting procedures.

All the examined specimens showed the fcc solid-solution phase only (*i.e.*, the γ phase in the stainless steel and the α phase in the gold alloy); in particular, the peaks of the ε and α' martensitic phases were never detected in the stainless steel specimens. In addition, the XRD did not show remarkable variations of the relative peak intensities in both the stainless steel and the gold-alloy samples subjected to explosions under different conditions: the 111 and 200 reflections were always the first and second most intense (except in one case), and the relative variations were generally less than 30 pct. It was not possible to find a sound correlation between the intensity variations and the test parameters (charge and sample-to-charge distance). In any case, the results indicate that experimental tests did not induce strong texture changes in the samples.

Since AISI 304Cu has a low stacking fault energy, one would expect to find stacking faults in the deformed samples, but the low peak-position shifts allowed us to estimate that their density does not vary appreciably after explosions.[10] On the contrary, the stacking fault density of the gold-alloy specimens after the explosion, as estimated from the peak-position shift (using the method of Warren,[10] based on previous work by Paterson[11]) and with consideration of the difference in respect to the as-prepared sample (Figure 9), decreases with decreasing charge-to-target distance. This latter result can be rationalized only by hypothesizing that the stacking fault density of the melted and resolidified regions is lower than that of the original material (which had been rolled and annealed).

The peak profile of the gold-alloy samples showed an overall symmetric broadening (*i.e.*, a significant increase of the full width at half height; Figure 10) after the explosion, generally more important at the lower charge-to-target distances, a feature that can be qualitatively related to an increase in the dislocation density,

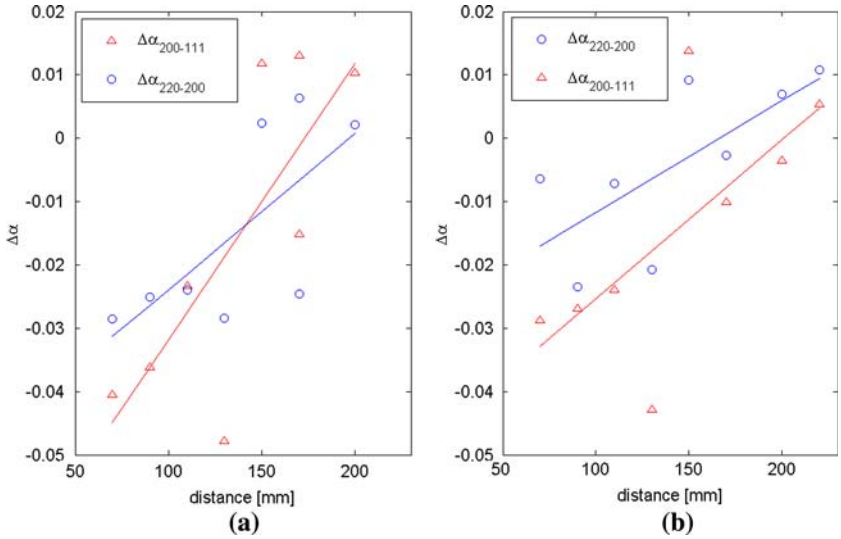

Fig. 9—(α) Differences in stacking fault density, calculated by the method of Warren,[10] between the as-prepared specimen and those subjected to explosion at increasing distances, for the (*a*) 670 and (*b*) 700 gold-alloy series. Results obtained from the 200 and 111, or 220 and 200, angular distances.

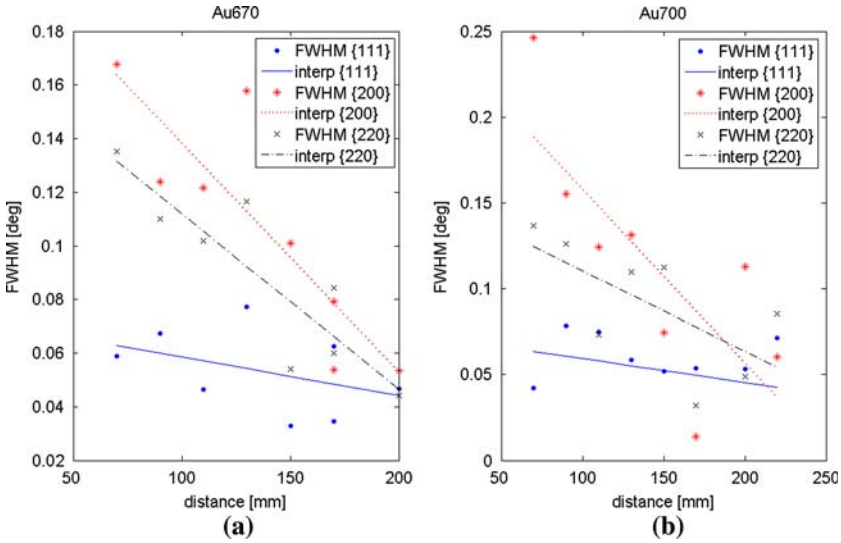

Fig. 10—Variation of the full-width at half-maximum of the 111, 200, and 220 diffraction peaks in the (*a*) 670 and (*b*) 700 gold-alloy series.

or to a lower mean crystallite size occurring in the melted and resolidified regions. Correspondingly, the density of dislocations of the gold-alloy samples (as calculated by the method of Williamson and Smallman[12] on the basis of the microstrain calculated by the method of Hall[13]), which is of the order of 10^9 cm^{-2}, shows moderately higher values in specimens subjected to explosions at the lower distances, and *vice versa*, to very large dispersion.

The stainless steel specimens do not show significant symmetric peak broadening, and the density of their dislocations (calculated with the same method) is similar in the surface layer of all the investigated samples, either as-annealed or exposed to explosions, lying in the vicinity of 10^8 cm^{-2} (comparable to the value of 3×10^8 cm^{-2} found by Sencer *et al.* on annealed AISI 304L specimens by TEM analysis[14]). Nevertheless, the stainless steel specimens showed an asymmetric broadening (Figure 11(a)) generally not observed in the gold-alloy case (Figure 11(b)); the broadening was localized in the low-intensity part of the peaks and along the tails, in particular, a feature that has been attributed to an increase in the density of the mechanical twins on the diffraction pattern.[10] The broadening generally increased with the increasing explosive charge and decreasing charge-to-specimen distance, *i.e.*, upon increasing the maximum applied pressure. For the same charge and charge-to-specimen distance, stainless steel specimens with a small grain size showed peaks that were more asymmetric than the large-grain ones.

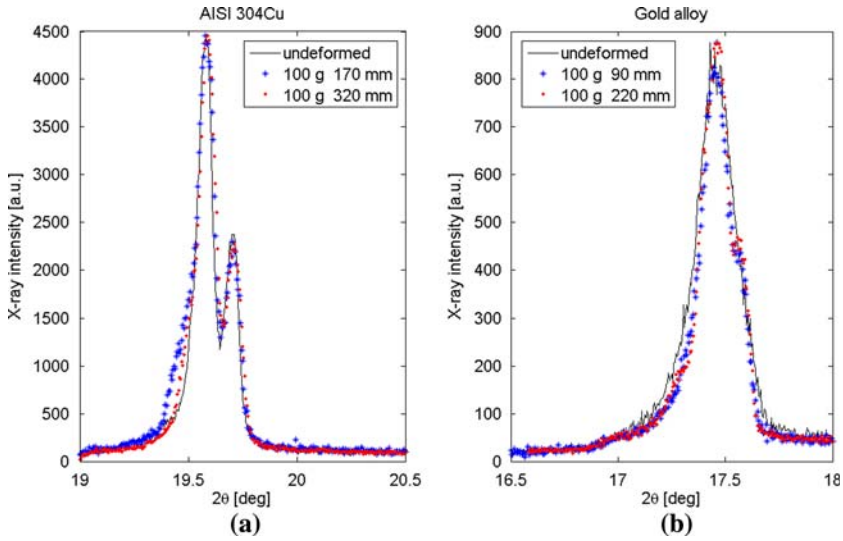

Fig. 11—Shape of the 111 reflection peak of samples, either as prepared or submitted to explosion. The peaks are scaled (in intensity) and shifted (in angle) to facilitate comparison: (*a*) stainless steel small-grain specimens and (*b*) gold-alloy 700 series specimens.

As an example, in Figure 11, the 111 peak profiles of specimens either as-prepared or subjected to explosions at selected distances are compared. In this figure, the peak intensities have been scaled and the peak positions shifted, to better compare the profile shapes. In the stainless steel case (Figure 11(a)), the profiles substantially overlap each other in the high-intensity part, whereas in the low-intensity part, the profiles of the blast-exposed samples exhibit a shape broadened toward low angles. The effect is more marked for the lowest charge-to-sample distance. The same features do not occur in the gold-alloy case (Figure 11(b)).

VI. DISCUSSION

A. *X-Ray Results and Nature of the Parallel Crystal Deformation Marks*

The nature of the parallel marks observed on the surface and in the cross sections of the blast-exposed samples cannot be determined from the OM observation only. In particular, the (unresolved) parallel marks observed on the surfaces are groups of parallel deformation steps that can be attributed to the interception of the (previously polished) surface by groups of either parallel slip planes or parallel twin planes, or a combination of both. The similar marks observed in the section are due to local differences of etching sensibility; they can also be attributed either to groups of parallel mechanical twins (because lattice regions located between successive twin planes generally have different crystallographic orientations and, therefore, can be differently etched), or to slip bands (because the latter are also bands of higher dislocation density, yielding a deeper etch), or to a combination of both. However, it is possible that the present etching technique results in greater evidence of mechanical twins than of slip (or cross-slip) in the cross section.

In the case of the stainless steel samples, the XRD analysis showed an asymmetric peak broadening that can be explained by the occurrence of mechanical twinning in the examined surface layer;[10] the same analysis demonstrated that the density of dislocations was not significantly increased, as it would be if significant slip deformation had occurred. Therefore, it is inferred that the parallel marks noted here (at and above the macroscopic deformation thresholds) were mainly due to mechanical twins.

On the contrary, in the case of the gold-alloy specimens, the XRD results were significantly influenced by the properties of the melted regions, and therefore do not offer an equally valuable contribution to the elucidation of the modes of the microscopic deformations of the original (unmelted) material. Nevertheless, the moderate increase in the average dislocation density (which occurs notwithstanding the probable reduction of the dislocation density of the melted regions) and the substantial absence of asymmetric peak broadening allow us to hypothesize that the microscopic deformation, and thus the parallel marks observed on the specimens' surfaces, are mainly due to slip planes (or possibly slip bands).

By comparing the results outlined in Table VIII, it is apparent that the difference between the surface and section thresholds is much larger in the gold alloy than in the stainless steel. In the stainless steel case, since it has been concluded that the microscopic deformation occurs by mechanical twinning and, moreover (on the basis of the earlier comments), since mechanical twins should be evidenced both in the surface and in the cross sections, the difference between the surface and section thresholds must be attributed to a different sensibility of the two experimental sequences to the same twinning phenomenon. In the gold-alloy case, instead, the much larger difference between the surface and section thresholds can be explained by hypothesizing that the slip mechanism primarily responsible for the microscopic deformation is clearly evidenced by the surface relief but

not by the cross-section etch, and that the cross-section parallel marks may be due to twins, which can be evidenced by etching and which may offer a minor contribution to the microscopic deformation (as opposed to slip) at the higher stress levels only, or to slip bands, which also may become evident in the etched section when the slip deformation is more intense.

Considering that the typical values of the critical shear stress for slip at low deformation rates, $\tau_{c,sl}$, vary from 10^{-4} to 10^{-5} G, where G is the shear modulus, the critical shear stress for slip can vary from 0.3 to 3 MPa in the case of the examined gold alloy, and from 0.7 to 8 MPa in the case of austenitic stainless steels, as AISI 304Cu. Thus, at low deformation rates, the critical shear stress for slip is lower for the gold alloy than for the austenitic stainless steel. On the contrary, the critical shear stress for twinning, $\tau_{c,tw}$, is higher for the gold alloy, as a consequence of its higher stacking fault energy. At increasing deformation rates, the critical shear stress for twinning does not vary significantly, whereas the critical stress for slip increases; thus, at high deformation rates, the critical shear stress for twinning can become lower than the critical shear stress for slip, and twinning can occur instead of slip. In the present case, it can be hypothesized that the $\tau_{c,tw}$ of the stainless steel is lower than the corresponding $\tau_{c,sl}$, and so twinning takes place, whereas the $\tau_{c,tw}$ of the gold alloy is comparable to or higher than the corresponding $\tau_{c,sl}$. Therefore, in the gold-alloy case, the deformation is mainly by slip, with a possible minor contribution by twinning, which will be further explored with a series of TEM observations.

B. *Detection of Blast-Related Twins vs Reduced Distance*

Since the examined fcc alloys at low deformation rates are known to deform by slip (or cross-slip) and, moreover, in the present set of experiments with small explosive charges, the occurrence of twinning has been recognized in the stainless steel, and possibly in the gold alloy (at least in certain overpressure, or charge-to-target distance, ranges, and pending further TEM studies), a forensic science criterion for recognizing the nature of an unknown event can be developed on the basis of the observation of mechanical twins in fcc alloy objects.[5]

In the AISI 304Cu stainless steel, which is characterized by a low stacking fault energy, a large prevalence of mechanical twins (as opposed to slip) can be observed in objects exposed to an explosion; if the original surfaces were sufficiently smooth, it may be possible to observe the surface parallel marks due to this phenomenon by OM, and to determine their nature by XRD analysis, at reduced distances larger than about 0.3 $m \cdot kg^{-1/3}$, when no macroscopic deformation occurs, and up to a maximum reduced distance of about 0.5 $m \cdot kg^{-1/3}$.

In the 18-carat-gold alloy, which has a higher stacking fault energy, the hypothesized mechanical twins may occur alongside a prevalent cross-slip deformation phenomenon only at reduced distances on the order of 0.2 $m \cdot kg^{-1/3}$ or lower, at which the macroscopic deformation is still sensible and relevant surface melting can also occur. In this case, the surface XRD analysis may not be conclusive because of the presence of surface melting areas, and the direct examination of the exposed surfaces by OM (if the original surfaces were sufficiently smooth) may not allow us to distinguish between parallel crystal deformation marks, due to slip and to twinning. The TEM studies may, therefore, be necessary to establish whether the parallel and crossed marks eventually observed in the cross section are mechanical twins and, thus, provide a proof of the fact that a gold-alloy object was subjected to a shock wave.

C. *Apparent and Microscopic Twinning Stresses*

In the stainless steel case, the τ_{max} values reported in Table VIII can be regarded as the apparent shear stresses that can cause an observable (depending on the observation method) amount of twinning in blast-exposed specimens. Therefore, they can be compared with the microscopically determined twinning shear stresses, $\tau_{c,tw}$, defined as the shear stress that can initiate twinning if applied in the more favorable crystallographic planes and directions and that can be evaluated from the literature. A similar comparison can be performed also for the 18-carat-gold alloy, although in this latter case, the occurrence of twins has not been definitely proven and the apparent τ_{max} values reported in Table VIII were not completely valid.

From the present results and hypotheses, the apparent shear stress for twinning can be evaluated as being on the order of 13 MPa (surface threshold) or 21 MPa (section threshold) for the stainless steel, and on the order of 23 MPa (section threshold, larger esteem) for the gold alloy (the surface threshold of the gold alloy is not considered here, because it has been hypothesized to be largely influenced by the slip deformation).

In the gold-alloy case, the values of $\tau_{c,tw}$ originally published by Suzuki and Barrett[15] for a Au-Ag alloy of various compositions are adopted as a reference for the present gold alloy in the absence of more specific measurements (*i.e.*, by neglecting the influence of Cu and by considering that $\tau_{c,tw}$ varies only slightly with the Au alloy content in the presently relevant range[15]); a value of 93 MPa is thus obtained.

In the AISI 304Cu case, a more precise estimate of $\tau_{c,tw}$ may be obtained on the basis of the stacking fault energy, γ_{sf}, by the use of relationships proposed by Suzuki and Barrett,[15] by Remy and Pineau,[16] or by Firrao *et al.*[1] The appropriate value for γ_{sf} was determined by the formulas proposed by Rhodes and Thompson[17] for AISI 304-type steels; the contribution of copper was evaluated taking into account the suggestions of Choi and Jin,[18] who based their reasoning on calculations by Inakazu *et al.*[19] Thus, a γ_{sf} value of 31 ± 8 mJ/m^2 was obtained;[20] with this value of γ_{sf}, the relationship by Firrao *et al.*[1] yields a $\tau_{c,tw}$ value of 69 MPa. Larger values are obtained by the use of the other two relationships.

Therefore, both in the gold-alloy and in the stainless steel cases, and even by adopting in the latter case the minimum acceptable value of γ_{sf}, the apparent twinning stress obtained from the analysis of the present set of

experiments and from the hypotheses already mentioned is much lower than the resolved twinning stress $\tau_{c,tw}$, as obtained from previous writings.

Therefore, the influence of other effects in addition to the peak pressure have to be taken into account, to understand fully the twinning phenomenon in metals under exploding charges. A sizable contribution to shear stresses may come from the constrained dilatation originating on the upper portion of the specimens from the temperature wave, which rapidly annihilates within the samples at the distances corresponding to the detectability limits. With additional research, the issue is being explored further.

VII. CONCLUSIONS

A series of explosions of small 50- and 100-g plastic-explosive charges (TNT equivalents are 54.5 and 109 g) were performed at charge-to-target distances in the 65- to 815-mm range, employing as targets 3-mm-thick disks consisting either of the AISI 304Cu austenitic stainless steel, with a 60- and 32-μm average grain size, or of an 18-carat-gold alloy, with a 55- and 45-μm average grain size. The following facts were ascertained and the ensuing conclusions drawn.

1. Melting of the surface layer happens in most gold-alloy specimens, but only at the shortest distances in the stainless steel.
2. Macroscopic deformations are very limited and are not found for distances exceeding 160 mm for the stainless steel samples tested with 50- or 100-g charge explosions, and for distances exceeding 170 mm for the gold-alloy samples tested with 100-g charge explosions.
3. In the stainless steel case, crystal atom order alterations mainly consist of extensive mechanical twinning, as evident on the exposed surface and in a discontinuous cross-section layer bordering the exposed surface; on the other hand, in the gold-alloy case, multiple cross-slip phenomena are probably the most frequent source of the crystal deformation parallel marks evident on the exposed surface, whereas the hypothesized occurrence of mechanical twins at the higher stresses requires further studies.
4. The XRD analysis was most useful in demonstrating the presence of mechanical twins in the stainless steel specimens exposed to the blast waves; in the gold-alloy case, the interpretation of the XRD results was less conclusive, because of the influence of the surface melted areas.
5. Mechanical twins were identified on the surface and the cross section of the stainless steel specimens, and their presence was thought to offer a possible explanation of some features observed on the surface and cross section of the gold-alloy specimens; mechanical twins can be considered as proof of the occurrence of a shock wave.
6. By a series of tests with sensor-instrumented targets, explosion peak pressures were measured and employed to calculate the maximum shear stresses, τ_{max}, applied at the exposed surfaces by using the elasticity hypothesis, which is valid when macrodeformations are absent. For each alloy, the τ_{max} values computed at the limiting optical microscopy detectability distance were substantially equal for all the experimental series and were compared with the critical resolved shear stress for twinning, $\tau_{c,tw}$, which was much higher both in the stainless steel and in the gold-alloy case.
7. To explain the difference between τ_{max} and $\tau_{c,tw}$, other effects, like constrained surface dilatation due to temperature waves rapidly disappearing in the bulk, have to be taken into account.

ACKNOWLEDGMENTS

The financial support of the Italian Ministry of Education, University, and Research, through the Progetto di Rilevante Interesse Nazionale Grant No. 2001094974, is acknowledged.

REFERENCES

1. D. Firrao, G. Ubertalli, and E. Cordano: *Technol., Law Insur.*, 1999, vol. 4, pp. 23–30.
2. G.E. Dieter: in *Strengthening Mechanisms in Solids*, J.J. Harwood, ed., ASM, Cleveland, OH, 1962, pp. 279–340.
3. C.S. Smith: *Trans. AIME*, 1958, vol. 212, pp. 574–89.
4. M.A. Meyers and K.K. Chawla: *Mechanical Metallurgy: Principles and Applications*, Prentice-Hall, Englewood Cliffs, NJ, 1984, p. 536.
5. D. Firrao, G. Matteis, G. Scavino, G. Ubertalli, M.G. Ienco, G. Pellati, P. Piccardo, M.R. Pinasco, E. Stagno, G. Costanza, R. Montanari, M.E. Tata, G. Brandimarte, and S. Petralia: *Foren. Sci. J.*, 2006, vol. 51 (3), pp. 520–31.
6. D. Firrao, P. Matteis, G. Scavino, G. Ubertalli, M.G. Ienco, G. Pellati, P. Piccardo, M.R. Pinasco, E. Stagno, R. Montanari, M.E. Tata, G. Brandimarte, and S. Petralia: *Mater. Sci. Eng., A*, 2006, vol. 424, pp. 23–32.
7. H.L. Brode: *J. Appl. Phys.*, 1955, vol. 26, pp. 766–75.
8. J. Henrych: *The Dynamic of Explosion and Its Use*, Elsevier, Amsterdam, 1979.
9. S. Petralia: *Compendio di esplosivistica*, Mariperman, La Spezia, Italy, 2000.
10. B.E. Warren: *X-Ray Diffraction*, Addison-Wesley, Reading, MA, 1969, pp. 275–98.
11. M.S. Paterson: *J. Appl. Phys.*, 1952, vol. 23, pp. 805–11.
12. G.K. Williamson and R.E. Smallman: *Philos. Mag.*, 1956, vol. 1, pp. 34–35.
13. W.H. Hall: *Proc. Phys. Soc. London*, 1949, vol. A62, pp. 741–43.
14. B.H. Sencer, S.A. Maloy, and G.T. Gray: *Acta Mater.*, 2005, vol. 53, pp. 3293–3303.
15. H. Suzuki and C. Barrett: *Acta Metall.*, 1958, vol. 6, pp. 156–65.
16. L. Remy and A. Pineau: *Mater. Sci. Eng.*, 1976, vol. 26, pp. 99–107.
17. C.G. Rhodes and A.W. Thompson: *Metall. Trans. A*, 1977, vol. 8A, pp. 1901–06.
18. J.Y. Choi and W. Jin: *Scripta Mater.*, 1996, vol. 36, pp. 99–104.
19. N. Inakazu, H. Yamamoto, and M. Ishio: *J. Jpn. Inst. Met.*, 1984, vol. 48, pp. 71–78.
20. D. Firrao, P. Matteis, and C. Pozzi: *Acc. Sci. Torino–Mem. Sci. Fis. Ser.*, 2005, vol. 29, pp. 3–20.